The Electrochemical Society
Advancing solid state & electrochemical science & technology

OPEN ACCESS

Full-, Half-, and Symmetrical Cell Analysis of Lithium-Ion Battery Using Impedance and Nonlinear Frequency Response

To cite this article: Yan Ying Lee *et al* 2024 *J. Electrochem. Soc.* **171** 070543

View the article online for updates and enhancements.

Full-, Half-, and Symmetrical Cell Analysis of Lithium-Ion Battery Using Impedance and Nonlinear Frequency Response

Yan Ying Lee, Hoon Seng Chan, Julian Ulrich, André Weber, and Ulrike Krewer[z]

Karlsruhe Institute of Technology (KIT), Institute for Applied Materials—Electrochemical Technologies (IAM-ET), D-76131 Karlsruhe, Germany

This study presents an in-depth analysis of the cathode and anode of a commercial 18650 lithium-ion battery by comparing their dynamic behaviors systematically with that of two additional experimental cell setups: (i) full-cell in a three-electrode setup and (ii) symmetrical cathode and anode cells. The analysis involves subjecting the cells to electrochemical impedance spectroscopy, distribution of relaxation times, and nonlinear frequency response analysis at different state-of-charges. Our findings highlight the importance of analyzing the electrodes in all three setups. The impedance and nonlinear frequency response features of the full-cell are also observed in the electrode-resolved cells. Symmetrical cells exhibit stronger impedance and nonlinear responses compared to the commercial cell and the cell with reference electrode, yet they allow identifying contributions of the single cells without artifacts from inductive loops caused by the reference electrode. By correlating nonlinear signals and characteristic peaks across different cell setups, cathode and anode processes and their respective characteristic frequencies can be clearly identified.

Battery characterization is an essential aspect of the application of lithium-ion batteries (LiBs), which aims to achieve a better understanding of their operating and aging processes. Electrochemical impedance spectroscopy (EIS) stands as a widely employed characterization method, operating under the assumption that the system can be linearized in the selected operating point.[1] However, in electrochemical systems which typically exhibit nonlinear behavior, the application of EIS has limitations, as it cannot access information on nonlinear system dynamics.[2] In response to this challenge, nonlinear frequency response analysis (NFRA) has garnered attention in LiBs in recent years. NFRA is also known as nonlinear EIS (NLEIS). We recommend using NFRA and use it in this paper because it provides a more precise description.[2] This method emerges as a valuable tool, enabling the extraction of additional nonlinear information, on surface processes such as charge transfer kinetics, and degradation state.[3–5] In these studies, the experimental work was carried out on pouch cells with a NMC-622 cathode and a graphite anode, restricting the analysis to only full-cell, making it difficult to analyze the individual electrode processes at the cathode and anode. Although NFRA experiments have been performed on 18650 cell, the exploration of nonlinear responses for individual electrodes remains unexplored.[6]

Chan et al. delved into the NFRA of LiBs using experimental cells in a three-electrode setup, focusing primarily on investigating the relationship between the electrode's particle size distribution and the nonlinear responses.[7] Ernst et al. adopted a comparable approach by using NFRA to study the battery's nonlinearity during charging and discharging.[8] Their methodology involved the application of an alternating current of 2 mA superimposed on a direct current of 5 mA (approximately 1 C) to the experimental cells. The nonlinearities of the cells were therefore not measured in a steady state. In another study, Kirk et al. utilized NFRA of a commercial pouch cell for model parameterization, where the author focused on the analysis of the fundamental and second harmonics.[9]

To understand the behavior of battery materials,[10,11] parameterize battery models,[12,13] and investigate the aging of battery electrodes,[14–16] researchers often disassemble commercial batteries to construct experimental full-cells, half-cells, or symmetrical cells, and apply C-rate test and EIS to investigate the electrodes' processes. Full-cell and half-cell in two- and three-electrode configurations are commonly used for electrochemical characterizations.[17] The analysis of a single EIS spectrum in a two-electrode full-cell can be challenging due to the numerous processes originating from each electrode.[18] While the use of a reference electrode proves beneficial for purposes such as identifying impedance contributions from each component, careful attention must be paid to the chemical composition, geometry, and positioning of the reference electrode.[19] Conversely, electrochemical testing on symmetrical cells yields spectra devoid of interference from a different electrode, providing cleaner insights.[20] To our best knowledge, there exists an unexplored avenue in the literature regarding the separate experimental analysis of cathodic and anodic nonlinearities using NFRA in commercial cells and a systematic comparison of these with experimental cells.

In this contribution, we, therefore, explore the impedance and nonlinear responses of a commercial 18650 NMC-811/silicon-graphite cell to obtain a better understanding of the commercial lithium-ion batteries, the nonlinearities of its electrodes, and whether the dynamic behavior is similar or strongly changed between the different cell setups. Characteristic frequencies are identified and compared. We compare results from EIS, distribution of relaxation times (DRT), and NFRA of the commercial 18650 cell with various cell configurations: (i) experimental cell in full-cell configuration, (ii) half-cells (cathode/anode against lithium metal reference ring), and (iii) symmetrical cells. The study elucidates the additional information gained from nonlinear analysis.

Material and Methods

Commercial and experimental cells.—A fresh commercial cell (18650HG2, 3 Ah) manufactured by LG, with a cathode of NMC-811 and silicon-graphite anode was disassembled in an argon-filled glove box (O_2 and H_2O < 0.1 ppm). Using N-Methyl-2-pyrrolidone, active material was removed from one side of the harvested cathode in the glovebox. For the anode, the active material was removed with dimethyl sulfoxide under atmospheric conditions and subsequently dried in a vacuum oven at 120 °C for 12 h. Circular disks measuring 18 mm in diameter were then punched from the electrode rolls, followed by a rinsing step with dimethyl carbonate (DMC).

Experimental full-cells and symmetrical cells were built using PAT-Cells from EL-Cell GmbH. The PAT-Cell setup includes electrodes measuring 18 mm in diameter and a PAT-Core, which consists of a reusable polyether ether ketone insulation sleeve and a 220 μm thick polypropylene (PP) fiber/polyethene (PE) membrane separator. Additionally, the PAT-Core of the experimental full-cell includes a reed contact and a lithium metal reference ring. For electrolyte, we used 103 μl mixtures of ethylene carbonate (EC) and DMC with a ratio of 1 : 1 (v/v) and 1 M lithium hexafluorophosphate
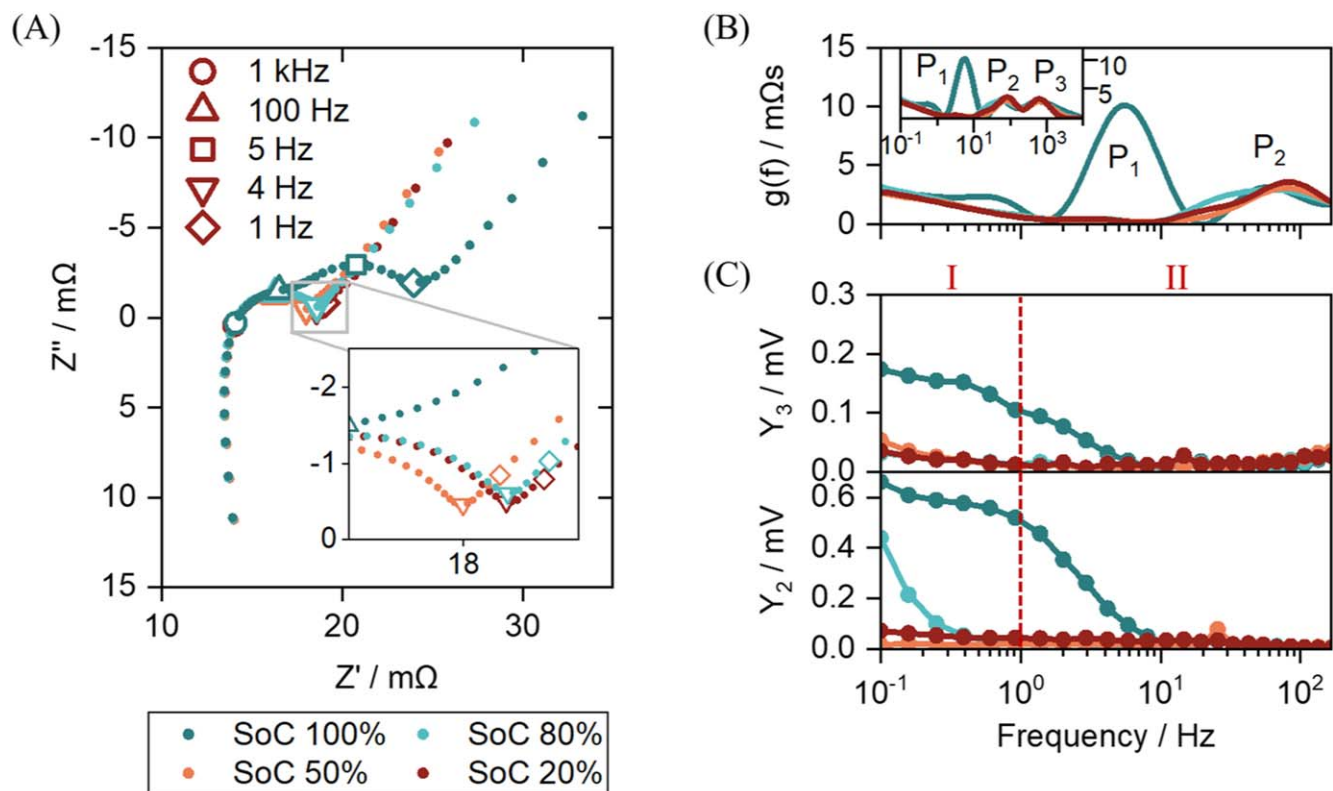
[z]E-mail: ulrike.krewer@kit.edu

Figure 1. (A) EIS, (B) DRT with peaks P_1 to P_3, (inset: complete frequency range), and (C) NFRA of the commercial 18650 cell measured at different SoCs and 23 °C. The vertical dashed line in (C) indicates the separation between regions I and II.

(LiPF$_6$). The experimental and full-cells were assembled in an argon-filled glovebox (O$_2$ and H$_2$O < 0.1 ppm).

After cell assembly, a cell formation process was carried out with two 0.1 C constant current cycles and a third 0.1 C constant current-constant voltage (cut-off current at 0.05 C) cycle. For assembling symmetrical cells, the positive and negative electrodes were prepared by fully charging cathode/Li and anode/Li cells, followed by a discharging step with 0.1 C to the desired state-of-charge (SoC). The formation cycles and SoC adjustment were performed using a battery cycler BaSyTec CTS LAB XL in a climate chamber (ESPEC EUROPE GmbH, SU 642) at 25 °C. After the SoC adjustment, the cells were disassembled in the glove box, and the electrodes were rinsed in DMC, dried, and reassembled into symmetrical cells. No formation steps were carried out on the symmetrical cells. Instead, the cells were kept in a climate chamber for 12 h at 25 °C to allow proper wetting of the separator. Preparing anode symmetrical cells was especially challenging because multiple handling of the negative electrodes caused the coating to flake off easily. Table I summarizes the information on the cells that were analyzed.

Electrochemical characterization.—We carried out EIS and NFR measurements using a Zahner Zennium Potentiostat at 23 °C (Memmert TypIPP14_S0 climate chamber) and four different SoCs of 100%, 80%, 50%, and 20%. For each cell configuration, both measurements were performed one time at the respective SoC. We conducted separate EIS and NFR measurements as the high excitation amplitudes for NFRA may change the amplitude of the impedance response.

To perform the NFR measurement of the 18650 cell, we connected a Zahner Power Potentiostat (PP241) to the Zennium to provide the high current required. Both EIS, and NFR measurements were conducted in galvanostatic mode. For EIS, an excitation current of 0.5 A was applied, and the frequency range was set between 10 mHz and 10 kHz for the commercial cell. For the experimental cell,

the excitation current was 0.5 mA, and the frequency range spanned from 10 mHz to 1 MHz. In NFRA, higher excitation amplitudes of 5 A were used, and a narrower frequency range between 100 mHz and 10 kHz was employed for the commercial cell. For the experimental cell, an excitation current of 50 mA was applied, and the frequency range covered 100 mHz to 1 kHz. The frequency range for NFR measurements was narrower to prevent any drift of the state of the cell. To adjust the SoC of the 18650 cell and experimental full-cell, we discharged a fully charged cell with 0.1 C over a specified duration, depending on the desired SoC, and rested the cells for at least two hours before performing the characterization measurements.

For the NFR measurements, harmonic responses from the second to ninth harmonic, Y_{2-9}, were recorded by the Zahner Zennium Potentiostat, representing the amplitude of the voltage response. Only the second, Y_2, and third harmonic, Y_3, had sufficiently high signal-to-noise ratios. Thus, we focused the analysis on these. We followed the steps that were recommended in the literature to ensure the quality of the response signals as described in.[7] The unreliable NFR data region is greyed out. DRT analysis was performed using the in-house developed "All-Fit"-tool in MATLAB, where a regularization parameter of $\lambda = 0.001$ was selected.

Results and Discussion

Investigation of 18650 cell.—We start our analysis with EIS, DRT and NFR analysis of the commercial cell. Figures 1A and 1C display EIS and NFRA for SoC 100%, 80%, 50%, and 20%. The highest impedance and nonlinearities occur at SoC 100%. While differences in impedance at lower SoCs are quite small, a trend can be identified with impedance being lowest at SoC 50%, followed by SoC 20%, and 80%. This observed variation in impedance can be attributed to the different degrees of intercalation and deintercalation of lithium-ions within the respective electrodes. As the electrodes approach highly intercalated and deintercalated states, respectively, the intercalation and deintercalation processes become progressively
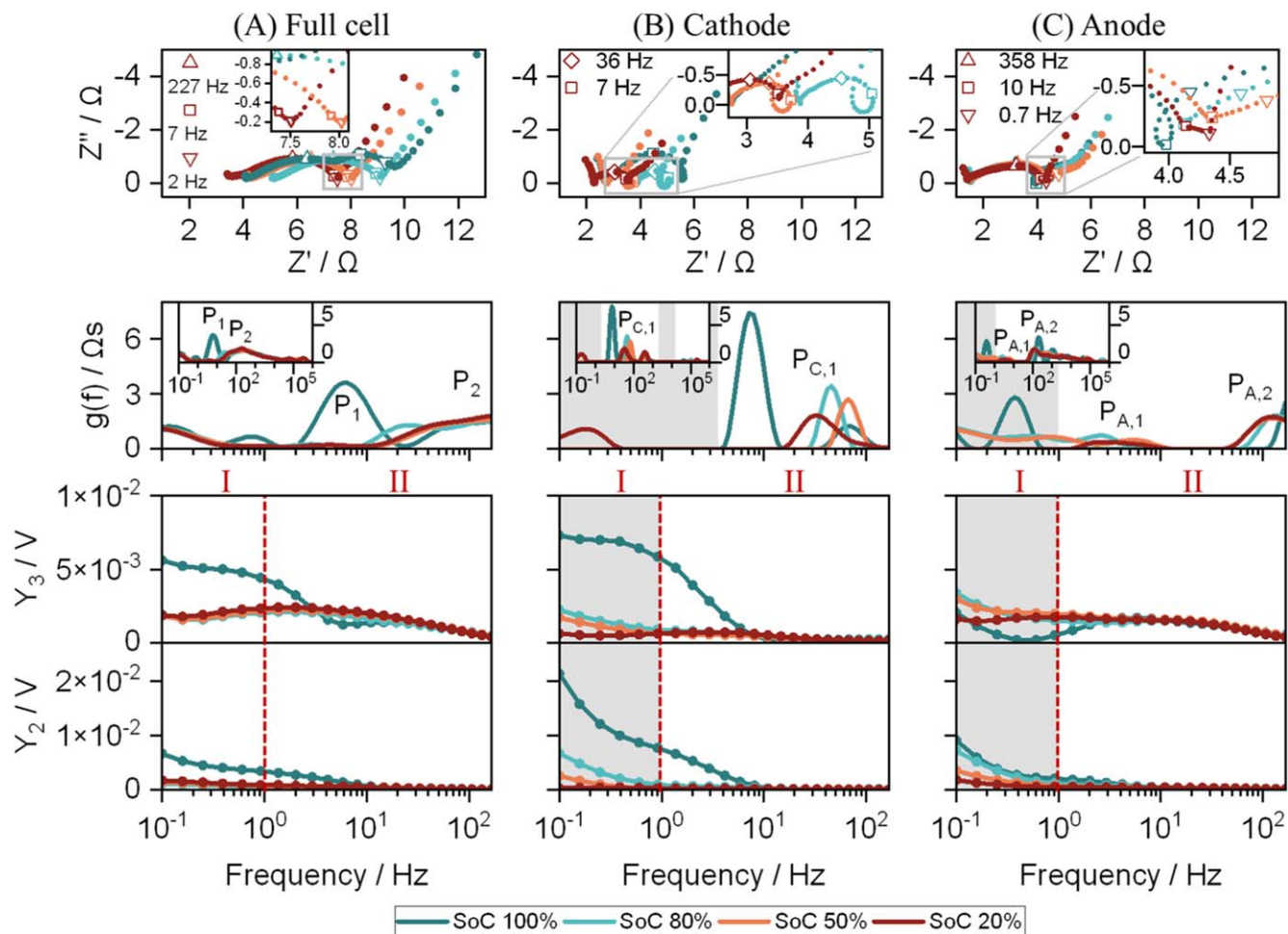
Figure 2. Top to bottom: EIS, DRT with characteristic peaks, P, (inset: complete frequency range), and NFR spectra with indicated frequency regions I and II of the experimental cell in a three-electrode setup measured at different SoCs and 23 °C. (A) full-cell, (B) cathode measured via lithium reference ring, and (C) anode measured via lithium reference ring. Shaded regions indicate data regions where data reliability may be compromised.

impeded, leading to greater impedance at both, the lower and higher ends of the SoC spectrum. At SoC 100%, the impedance spectrum shows an additional semicircle around 1 Hz to 10 Hz, which is not visible for other SoCs. The DRT analysis in Fig. 1B reveals three distinct peaks at SoC 100%. P_3, situated at high frequencies around 1 kHz, is attributed to contact resistance, while P_2 and P_1, positioned in the medium and lower frequency regions, are associated with charge transfer processes at the electrodes. It is important to note that, due to the absence of a reference electrode, we cannot definitively ascertain whether the peaks correspond to cathode or anode processes. At lower SoCs, besides the high-frequency peak, P_3, we observe only the peak at medium frequencies around 100 Hz, P_2. This suggests an overlap of the two electrode processes, contributing to the appearance of a single semicircle in impedance spectra at these lower SoCs. In the subsequent section, we explore the cathode and anode processes employing an experimental cell equipped with a reference electrode.

Investigation of experimental full-cell with a reference electrode.—The use of an inappropriate reference electrode design such as a lithium metal ring can result in errors in the spectra as investigated by Ender et al.[21] This is especially visible by the presence of the inductive loop at low frequency regions. Nonetheless, such configuration was applied in this study for a rough correlation of the DRT peaks to the cathode and anode, respectively. Attempts to consider these inductive loops by a negative peak in the DRT[22] were avoided as these loops are in the mid-frequency range and can hardly be separated. Instead, mainly

the amplitude and characteristic frequencies at loop-free regions are interpreted. Furthermore, in contrast to symmetrical cells, the interactions between the electrodes remain identical to that of the commercial full-cell.

Figure 2A presents the impedance spectra of an experimental full-cell. In line with observations from the 18650 cell, the highest impedance is observed at SoC 100%, with two separate electrode processes. The frequencies at which the maximum points occur for the medium and low-frequency semicircles are approximately 200 Hz and 10 Hz, respectively. This is similar to the frequencies in the commercial 18650 cell (see Fig. 1A). By examining the cathode impedance spectra depicted in Fig. 2B, we can affirm that the low-frequency semicircle in the spectra of the full-cell corresponds to the cathode. This affirmation is substantiated by the characteristic frequency observed at 7 Hz in the SoC 100% spectrum. Conversely, the anode impedance spectra, shown in Fig. 2C, consistently exhibit a characteristic frequency at around 300 Hz for all SoCs. Consequently, it is plausible that the medium frequency semicircle in the full-cell pertains to the anode process. In the low frequency range between 1 Hz to 10 Hz of the anode half-cell, we can see a much smaller semicircle in the impedance spectra, and peak $P_{A,1}$ in the DRT. Upon comparing the DRT analysis of the full-cell (Fig. 2A) with that of its two electrodes (Figs. 2B and 2C), it becomes evident that the low-frequency peak of the full-cell spectrum, P_1 corresponds to the low-frequency peak of the cathode spectrum, $P_{C,1}$, particularly at SoC 100%. In the lower SoCs, the mid-frequency peak of the full-cell spectrum, P_2 may potentially result from overlapping contributions of $P_{A,2}$ and $P_{C,1}$. The sum of
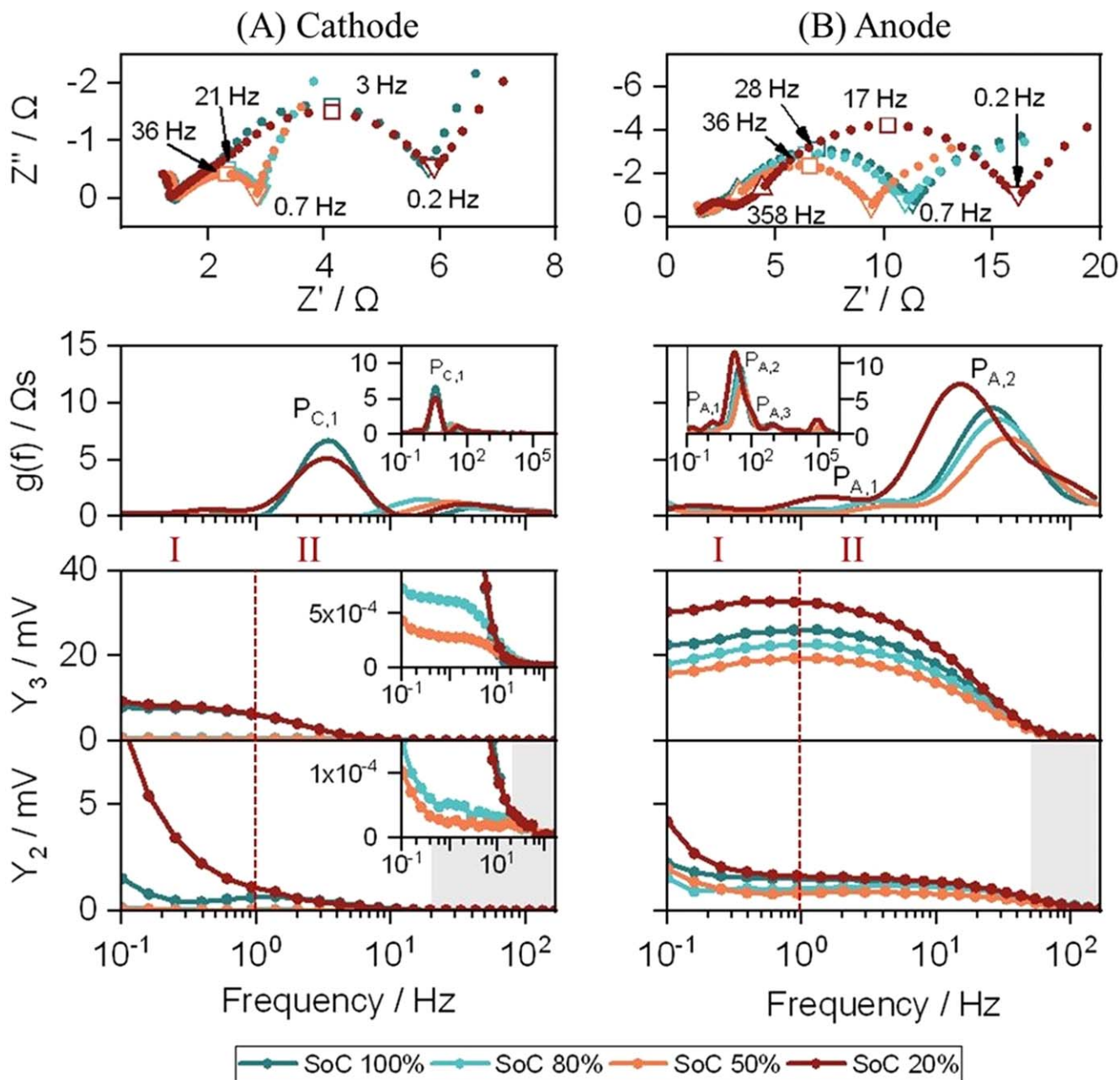
Figure 3. Top to bottom: EIS, DRT with characteristic peaks, P, (inset: complete frequency range), and NFR spectra with indicated frequency regions I and II for (A) cathode, and (B) anode symmetrical cells measured at varying SoCs and 23 °C. Values have been divided by two to signify the individual contribution of each electrode. Shaded regions indicate data regions where data reliability may be compromised.

the cathode and anode half-cell DRTs results in higher peaks compared to the full-cell DRT due to the inductive loops in the half-cells, which should produce a negative peak in the DRT. Since the DRT algorithm does not support negative peaks, this discrepancy arises between the summed half-cell DRT and the full-cell DRT. We acknowledge that the non-shaded regions are also impacted by this artifact, though likely only slightly. The low-frequency region is more significantly affected, with the EIS feature being strongly distorted. Consequently, this region is greyed out and excluded from the analysis. Furthermore, NFRA demonstrates its capability in process identification, notably in the amplitude of the third harmonic response, Y_3. It reveals two distinct levels of nonlinear behavior, with a transition occurring around 7 Hz. The high nonlinearities in the lower frequency range can be attributed to the cathode (Fig. 2B), while those at higher frequencies originate from the anode only (Fig. 2C). It should be noted that NFRA shows no nonlinearities in

the cathode spectra in the mid-frequency range. The weak nonlinear response in the mid-frequency range indicates that this is not a charge transfer process.

At SoC 100%, the contribution from the cathode is more prominent than that of the anode. This phenomenon arises because, at this SoC, the cathode is predominantly delithiated. Consequently, there is a noticeable increase in nonlinearities, particularly Y_3, which, as previously elucidated in[23] is sensitive to the rate of the charge transfer process. As the cell nears SoC 100%, the charge transfer process begins to decelerate due to lithiation saturation on the anode side and lithium-ion depletion on the cathode side. This results in a hindered charge transfer process, reflected in the increasing Y_3 values. Additionally, an asymmetry between intercalation and deintercalation kinetics in the cell is observed, indicated by notable amounts of the second harmonic, Y_2 for SoC 100%. This holds for the full-cell and the cathode spectrum. Asymmetry was

Table I. Information on the investigated cells.

Cell configuration	Electrode materials	Separator	Electrolyte
Commercial 18650 cell (LG18650HG2)	Cathode: NMC-811 Anode: Silicon-graphite	Unknown	Unknown
Experimental full-cell with lithium metal reference ring (Ca/Li/An)	Cathode and anode from 18650 cell	PP fiber/PE membrane Thickness: 220 μm	1 M LiPF$_6$ in EC:DMC 1:1 (v:v)
Symmetrical cathode cells (Ca/Ca)	2x cathodes from 18650 cell, cathodes were adjusted to SoCs of 100%, 80%, 50%, and 20%	PP fiber/PE membrane Thickness: 220 μm	1 M LiPF$_6$ in EC:DMC 1:1 (v:v)
Symmetrical anode cells (An/An)	2x anodes from 18650 cell, anodes were adjusted to SoCs of 100%, 80%, 50%, and 20%	PP fiber/PE membrane Thickness: 220 μm	1 M LiPF$_6$ in EC:DMC 1:1 (v:v)

shown in simulations to occur if the current-potential relationship is not point symmetric around open circuit potential, i.e. intercalation and deintercalation kinetics are different.[23] At SoC 100%, this seems to be the case and it is attributed to very little amount of lithium in the cathode, which aggravates delithiation.

Investigation of symmetrical cells.—Due to the artifacts in the spectra introduced by the reference electrode, quantitative data derived from these half-cells becomes uncertain. Consequently, we use the half-cell measurements mainly for a rough estimation of the characteristic frequencies and for attribution of features to single electrodes. In this section, we investigate the cathode and anode employing symmetrical cells. This setup allows us to explore the individual processes occurring at the positive and negative electrodes, free from the influence of mutual electrode interactions, and from the reference electrode-induced artifact. Note that the values have been divided by two to signify the individual contribution of each electrode.

The cathode impedance spectra in Fig. 3A exhibit a prominent semicircle, similar to the spectra observed for the cathode vs lithium reference cell, with the semicircle's radius strongly influenced by the SoC. This semicircle is attributed to the charge transfer process. Notably, the impedance of the cathode at SoC 100% and 20% is considerably higher compared to SoC 80% and 50%. In the cathode DRT analysis (Fig. 3A, a single peak $P_{C,1}$ is observed within the frequency range of 1 Hz to 100 Hz. $P_{C,1}$ not only exhibits an increase in amplitude but also shifts to lower frequencies at both SoC extremes. This shift can be attributed to the decrease or increase in the concentration of lithium in the cathode as it becomes very delithiated or lithiated, respectively, leading to a higher charge transfer resistance.[24] A noteworthy distinction in the symmetrical cell spectra is that the impedance at SoC 20% is stronger and occurs at slower frequencies. Even in the spectrum with the reference electrode, the peak at SoC 20% shifts to notably lower frequencies compared to SoC 80% and 50%. This effect is more pronounced in the symmetrical cells. Furthermore, as depicted in Fig. 3A, SoC 100% and 20% exhibit a significantly stronger nonlinear behavior in the frequency range below 10 Hz. The cathode NFR spectrum shows a sharp increase in the Y_3-signal, with notable contributions below 10 Hz (Region II), signifying the onset of a reaction process. With nonlinearities present, the response in this range can be unambiguously attributed to charge transfer processes at the cathode. Additionally, Y_3, reflecting charge transfer kinetics, is significantly more pronounced at SoC 100% and 20%, aligning with the impedance findings. Moreover, there is a noticeable increase in Y_2 below 10 Hz, specifically for SoC 100% and 20%, signifying asymmetric intercalation and deintercalation kinetics. Y_2 exhibits an exponential increase for all cases in the frequency range between 0.1 Hz and 1 Hz (Region I). This is attributed to slow diffusion processes, particularly in the solid material of the cathode, impacting kinetics asymmetrically. Simulations have validated that (solid) diffusion causes an exponential increase in Y_2 at the corresponding low frequencies.[23]

When analyzing the impact of SoC on anode impedance in Fig. 3B, we observe an SoC-dependent low-frequency semicircle around 1 Hz to 40 Hz, and a much smaller contribution at around 300 Hz. Notably, the impedance for the low-frequency semicircle is the highest at SoC 20%. DRT analysis of the anode reveals two low-frequency peaks, $P_{A,1}$ and $P_{A,2}$, and a high-frequency peak, $P_{A,3}$, with $P_{A,2}$ being notably larger than $P_{A,1}$ and $P_{A,3}$. The presence of two peaks in the low-frequency region (around 1 Hz to 50 Hz) suggests the possibility of two anode charge transfer processes. It may be possible that the taller $P_{A,2}$ is associated with the charge transfer at the graphite particles, while $P_{A,1}$ is related to the charge transfer at the silicon particles. This may also explain the observation of a process between 1 Hz to 10 Hz in the anode half-cell spectrum Fig. 2C. In the NFR spectra of the anode (Fig. 3B, a substantial increase in the third harmonic, Y_3, within the frequency range below 50 Hz (Region II) is identified. This frequency range closely aligns with that of $P_{A,2}$, indicating a correlation between this peak and Region II, suggesting their association with the anode charge transfer process. Literature reports a higher exchange current density for graphite (around 2.3 mA cm^{-2})[25] compared to silicon (around 0.1 mA cm^{-2}).[26,27] However, the contribution of charge transfer resistance and nonlinearity for silicon is significantly smaller, likely due to the very small amount of silicon active material in the electrode. As we move beyond 100 Hz, the nonlinearity diminishes to zero, indicating the presence of a linear or weakly nonlinear process in the higher frequency region. $P_{A,3}$ is attributed to the ionic transfer at or through the SEI layer, as it is a fast process and demonstrates characteristics of a linear process.[3] It is worth noting that, in contrast to the cathode, changes in the SoC have a minimal impact on the time constant of the anodic charge transfers. When we compare the impedance of the anode in the symmetrical cell to that of the anode half-cell, a notable observation is that the impedance in the symmetrical cell is two to three times higher than in the half-cell configuration. This difference in impedance could potentially be attributed to surface change on the anode that occurred during the reassembly process, which did not contain a further formation procedure. Despite our diligent efforts to exercise caution during the reassembly process, it is important to note that the anode's active material is inherently more delicate, also because the SEI will strongly impact charge transfer, which may explain this phenomenon.[28]

In a symmetrical cell, we should expect that the Y_2-signal ideally becomes zero. This arises from the two nominally identical electrodes that should exhibit identical voltage responses to the sinusoidal excitation with a π phase-shift. Consequently, the Y_2-signals from both electrodes would annihilate each other. However, this anticipated symmetry is not upheld as we see weak but noticeable Y_2 contributions in Figs. 3A and 3B. The full exploration of this deviation from the expected behavior is outside the intended scope of this paper.

The examination of symmetrical cells has provided valuable insights, leading to several key observations. Firstly, the cathodic charge transfer process exhibits a notably higher sensitivity to

variations in the SoC compared to the anodic process. Secondly, both the cathode and anode charge transfer reactions occur within the same frequency range.

Conclusions

The comparative analysis of a commercial cell and corresponding experimental cell configurations through impedance spectroscopy, DRT analysis and NFRA enabled the deconvolution of the electrochemical processes in the cathode and anode. For the first time, electrode-resolved NFR spectra were recorded and analyzed using symmetrical cells. The spectra of the experimental full-cell, which featured a reference electrode, revealed several peaks in the DRT that could be attributed to the cathode and anode processes. To address substantial artifacts caused by the reference electrode in both the cathode and anode spectra, we conducted additional analyses using symmetrical cells. However, challenges also exist in the symmetrical cells: we observed a higher charge transfer resistance than for the cells with reference electrode, as well as notable contributions of the second harmonic, which was supposed to be zero. We attribute these to the complex cell manufacturing of symmetrical cells.

The physical background of the processes deconvoluted by DRT analysis could be resolved by NFRA, which allows us to distinguish between linear and nonlinear processes. The study has unveiled a noteworthy contrast in the nonlinear response of the commercial cell, which appears weak except at SoC 100%. Even when subjecting the cell to a high excitation rate of nearly 6 C, there was a negligible magnitude of the response signals. This behavior may be specific to the 18650 cell. In contrast, experiments using full-, half-, and symmetrical experimental cells revealed distinct nonlinearity responses. This underscores the significance of analyzing the cathode and anode using symmetrical cells to effectively understand the behavior of the commercial lithium-ion full-cell. While this approach can be laborious, we can single out the interaction between the cathode and anode, thus, enabling us to obtain a clearer picture and a deeper understanding of the processes that are taking place in the respective electrodes.

Furthermore, the application of NFRA has emerged as a valuable tool for deciphering the origins of nonlinear behaviors in batteries. By comparing characteristic peaks in DRT with the frequency ranges of various processes analyzed using NFRA, we can accurately discern the time constants of processes inside the cell. NFRA proves particularly useful in distinguishing between the charge transfer process and transport across the SEI due to the linearity of the latter process, which is otherwise challenging to differentiate using linear characterization methods, as the processes take place within similar frequency ranges. In the context of this study, the combined analysis methodology was applied to a Li-ion battery featuring NMC/Si-G chemistry for process identification. It is important to note that batteries with different chemistries or capacities may exhibit processes in different frequency regions. We anticipate that this method is also applicable to other battery systems, provided there are no additional artifacts.

Acknowledgments

ORCID

Yan Ying Lee ⓘ https://orcid.org/0000-0003-4105-5246
Hoon Seng Chan ⓘ https://orcid.org/0000-0002-9507-1957
André Weber ⓘ https://orcid.org/0000-0003-1744-3732
Ulrike Krewer ⓘ https://orcid.org/0000-0002-5984-5935

References

1. D. Andre, M. Meiler, K. Steiner, C. Wimmer, T. Soczka-Guth, and D. U. Sauer, *J. Power Sources*, **196**, 5334 (2011).
2. T. Vidaković-Koch, T. Miličić, L. A. Živković, H. S. Chan, U. Krewer, and M. Petkovska, *Current Opinion in Electrochemistry*, **30**, 100851 (2021).
3. N. Harting, N. Wolff, F. Röder, and U. Krewer, *Electrochim. Acta*, **248**, 133 (2017).
4. N. Harting, N. Wolff, and U. Krewer, *Electrochim. Acta*, **281**, 378 (2018).
5. N. Harting, N. Wolff, F. Röder, and U. Krewer, *J. Electrochem. Soc.*, **166**, A277 (2019).
6. N. Wolff, N. Harting, M. Heinrich, F. Röder, and U. Krewer, *Electrochim. Acta*, **260**, 614 (2018).
7. H. S. Chan, L. Bläubaum, D. Vijayshankar, F. Röder, C. Nowak, A. Weber, A. Kwade, and U. Krewer, *Batteries & Supercaps*, **6**, e202300203 (2023).
8. S. Ernst, T. P. Heins, N. Schlüter, and U. Schröder, *Front. Energy Res.*, **7**, 550 (2019).
9. T. L. Kirk, A. Lewis-Douglas, D. Howey, C. P. Please, and S. Jon Chapman, *J. Electrochem. Soc.*, **170**, 10514 (2023).
10. B. Rowden and N. Garcia-Araez, *Energy Reports*, **7**, 97 (2021).
11. C. H. Chen, J. Liu, and K. Amine, *Electrochem. Commun.*, **3**, 44 (2001).
12. C.-H. Chen, F. Brosa Planella, K. O'Regan, D. Gastol, W. D. Widanage, and E. Kendrick, *J. Electrochem. Soc.*, **167**, 80534 (2020).
13. R. Scipioni, P. S. Jørgensen, C. Graves, J. Hjelm, and S. H. Jensen, *J. Electrochem. Soc.*, **164**, A2017 (2017).
14. P. Röder, B. Stiaszny, J. C. Ziegler, N. Baba, P. Lagaly, and H.-D. Wiemhöfer, *J. Power Sources*, **268**, 315 (2014).
15. B. Stiaszny, J. C. Ziegler, E. E. Krauß, M. Zhang, J. P. Schmidt, and E. Ivers-Tiffée, *J. Power Sources*, **258**, 61 (2014).
16. R. Weber, A. J. Louli, K. P. Plucknett, and J. R. Dahn, *J. Electrochem. Soc.*, **166**, A1779 (2019).
17. R. Nölle, K. Beltrop, F. Holtstiege, J. Kasnatscheew, T. Placke, and M. Winter, *Mater. Today*, **32**, 131 (2020).
18. J. Moškon and M. Gaberšček, *Journal of Power Sources Advances*, **7**, 100047 (2021).
19. R. Raccichini, M. Amores, and G. Hinds, *Batteries*, **5**, 12 (2019).
20. Z. Yan, *J. Electrochem. Soc.*, **170**, 20521 (2023).
21. M. Ender, A. Weber, and I.-T. Ellen, *J. Electrochem. Soc.*, **159**, A128 (2011).
22. A. Schiefer, M. Heinzmann, and A. Weber, *Fuel Cells*, **20**, 499 (2020).
23. N. Wolff, N. Harting, F. Röder, M. Heinrich, and U. Krewer, *Eur. Phys. J. Spec. Top.*, **227**, 2617 (2019).
24. S. Gantenbein, "Impedanzbasierte Modellierung von Lithium-Ionen Zellen und deren Degradationsverhalten." *Doctoral dissertation*, Karlsruhe Institute of Technology (2019), 10.5445/KSP/1000099175.
25. Y.-C. Chang, J.-H. Jong, and G. T.-K. Fey, *J. Electrochem. Soc.*, **147**, 2033 (2000).
26. J. Li, X. Xiao, F. Yang, M. W. Verbrugge, and Y.-T. Cheng, *J. Phys. Chem. C*, **116**, 1472 (2012).
27. T. Swamy and Y.-M. Chiang, *J. Electrochem. Soc.*, **162**, A7129 (2015).
28. T. Momma, T. Yokoshima, H. Nara, Y. Gima, and T. Osaka, *Electrochim. Acta*, **131**, 195 (2014).